



Influence of Mn^{2+} ions on the corrosion mechanism of lead-based anodes and the generation of heavy metal anode slime in zinc sulfate electrolyte

Chenmu Zhang^{1,2} · Ning Duan² · Linhua Jiang² · Fuyuan Xu² · Jin Luo³

Received: 6 November 2017 / Accepted: 30 January 2018 / Published online: 15 February 2018
© Springer-Verlag GmbH Germany, part of Springer Nature 2018

Abstract

The influence of Mn^{2+} ions on the generation of heavy metal anode slime during zinc electrolysis industry was extensively investigated using several electrochemical methods, electron microscope technologies, and particle size analysis. Results showed that the Mn^{2+} could obviously promote oxygen evolution reaction (OER) and thereby weaken oxidation efficiency of Mn^{2+} (η_{MnO_2}) and dissolution of Pb^{2+} . The significant improvement in kinetic parameters for OER was found in electrolytes of 1 and 3 g/L Mn^{2+} , but became unstable as the Mn^{2+} concentration increased to 10 g/L. This result was correlated with much different properties of oxide layers that its changes of microstructure are involved in, since it confirmed that the positive role of compact oxide layers in contributing to high corrosion resistance and activity for OER, but excessive Mn^{2+} , resulted in its micromorphology of overthickness and instability. Such differences resulted from the effect of the Mn^{2+} concentration fluctuation on kinetic rates of the nucleation growth process. The formation and adsorption of intermediate MnO_2-OH_{ads} identified as the controlled step for Mn^{2+} catalyzing OER was also recommended. The generation mechanism of anode slime was found to be changed in essence due to varying Mn^{2+} concentrations. In electrolyte of 1 g/L Mn^{2+} , results revealed that the root cause of excessive small suspended anode slime (around 20 μm) was the change of the initial pathway of Mn^{2+} electro-oxidation, whereas, it showed great improvement in the settling performance as the Mn^{2+} concentration was increased to 10 g/L. Considering the potential of optimizing Mn^{2+} concentrations as a cleaner approach to control anode slime, deepening the understanding of the impact mechanism of Mn^{2+} can provide new insights into intervention in the generation of anode slime.

Keywords Oxygen evolution reaction · Heavy metal · Anode slime · Cleaner approach

Introduction

In the zinc electrolysis industry, electrodeposition process is particularly sensitive to the presence of various metallic

impurities in the electrolyte (Zhu et al. 2017). Over the past decades, many scholars have conducted a large number of studies with regard to the effect of numerous impurities on zinc electrodeposition. Low concentrations of nickel (Zhang et al. 2009; Liu et al. 2012), cobalt (Cachet et al. 1999; Krause and Sandenbergh 2015), copper (Mureşan et al. 1996), antimony (Ivanov 2004; Alkatsev et al. 2015), iron (Lins et al. 2010; Adcock 2017), cadmium (Moradkhani et al. 2012), and germanium (Liu et al. 2011; Alkatsev et al. 2014) have been regarded not only as influential in the zinc electrodeposition efficiency of cathode but also make a difference in the characteristics of zinc product microcosmic morphology and cathodic polarization.

China now has a dominant role in electrolytic zinc production of which production capacity reached 5,610,000 tons in 2014. According to the mass balance analysis of wastewater (Xu et al. 2016), 1,889,448 tons of

Responsible editor: Bingcai Pan

✉ Ning Duan
duancaes@163.com

✉ Linhua Jiang
jlhcaes@163.com

¹ School of Materials Science and Engineering, Beijing Institute of Technology, Beijing 100081, China

² Technology Center for Heavy Metal Cleaner Production Engineering, Chinese Research Academy of Environmental Sciences, Beijing 100012, China

³ School of Environment, Tsinghua University, Beijing 100084, China

wastewater containing 113.49 tons of Pb^{2+} is generated and discharged into the environment. As is known to all, the lead-based anode is widely used in the zinc electrolysis industry on account of its high corrosion resistance and availability in acidic sulfate (Houlachi et al. 2015), whereas the Pb^{2+} is attributed to the inevitable dissolution of Pb-Ag alloy (Rerolle and Wiart 1995). For improving the corrosion resistance, Mn^{2+} is required as an essential factor in the zinc electrolysis process, which can be oxidized to form oxide layers on the anode surface (Lai et al. 2011; Mohammadi et al. 2013a). This oxide layer is considered to not only favor the corrosion resistance but also to reduce the overpotential of OER in sulfate acid electrolyte (Alamdari et al. 2012; Mohammadi et al. 2013b; Mohammadi and Alfantazi 2015; Jaimes et al. 2015).

Despite this oxide layer having so many positive effects, lots of heavy metal anode slime are also generated in the presence of Mn^{2+} . In China, on average, to produce 1 ton of zinc, 40–50 kg of anode slime containing about 10% of Pb is generated and enters the electrolysis system. Normally, anode slime of cell bottom pumped by vacuum suction tower is reused in the electrolyte preparation process for oxidizing iron impurities (Ivanov and Stefanov 2002). But, this recycling pattern causing the potential risk of Pb accumulation within the electrolysis system is always ignored. Moreover, superabundant anode slime on the anode surface will lead to increasing energy consumption and risk of short circuit, and the cleaning and removal of the anode slime of cell bottom will also cause intermittent stoppages during the production (Moats 2008). These problems have long existed and continue to plague the improvement of the zinc electrolysis industry. Although some proposals are directed towards replacing other anode materials, such as titanium-based anode and iron-based anode, they are limited by its performance stability and expensive production cost (Shrivastava and Moats 2009; Liu et al. 2013; Stefanov and Dobrev 2013). Actually, Mn^{2+} ions are always sourced from zinc ore and are also inevitably introduced into the electrolyte through the leaching process. Therefore, the oxidation of Mn^{2+} ions on the anode is unavoidable.

Therefore, an attempt to understand the role Mn^{2+} plays in the generation of anode slime becomes much more practical and feasible. Recently, the researches in this field have its limitation and have paid most of their attention to the effect of Mn^{2+} on energy consumption, cathodic current efficiency, and zinc product quality (Zhang and Hua 2009; Su et al. 2017). However, the potential heavy metal pollution caused by the generation of excess anode slime is ignored. The previous literatures have reported the key role the Mn^{2+} concentration plays in the change of oxide layer morphology (Mohammadi and Alfantazi 2015). But, less attention has been paid on the intrinsic relation between the oxide layer characteristics and the generation of anode slime, especially detailed impact analysis of the Mn^{2+} concentration in the field of the change of the anode slime quantity, distribution,

and morphology characteristics. Considering the large amount of electrolyte preparation requirements during zinc electrolysis industry, the optimization of Mn^{2+} concentrations means high potential in reducing resource consumption.

Considering the potential of optimizing Mn^{2+} concentrations as a cleaner approach in improving the generation of anode slime at source, our work focused on evaluating the effect of changes in Mn^{2+} concentrations on the OER behavior and microstructure of oxide layers obtained from zinc sulfate electrolyte during 10 days of electrolysis and investigating their internal relation with the properties of anode slime. Based on this view, we brought insight into the special understanding of the generation mechanism of heavy metal anode slime.

Experimental details

Reagents

The electrolyte used in this study was prepared with 45 g/L Zn^{2+} and 160 g/L H_2SO_4 ; Mn^{2+} ions were added into the electrolyte to get the desired solution composition. All reagents ($\text{ZnSO}_4 \cdot 7\text{H}_2\text{O}$, H_2SO_4 , and $\text{MnSO}_4 \cdot \text{H}_2\text{O}$) were guaranteed reagent grade to ensure the composition of the electrolyte was pure without introducing other heavy metal impurities.

Electrolysis

Small-scale anodic galvanostatic electrolysis was performed in a 5000-cm³ plexiglass cell in the absence and in the presence of various amounts of Mn^{2+} ions to keep the ion variations comparable. Two lead alloy samples (Pb-0.3% Ag-0.03% Ca-0.03% Sr) with geometric areas of 30 and 1 cm² were used as the anodes, and the corresponding aluminum sheets with the same areas with anodes were used as cathodes. In all cases, each designed experiment of Mn^{2+} ions galvanostatic electrolysis was performed in a constant temperature bath at 35 ± 1 °C, and the current density was held constant at 450 A/m² by a multi-channel DC power supply. Upon reaching specific electrolysis time points (0, 24, 48, 72, and 240 h), the cathode was removed from the cell to strip zinc products. Then, the new electrolyte and cathodes were replaced for the next 24 h of electrolysis. The anode samples were also immediately removed from the electrolytic cell and washed three times with the doubly distilled water, then prepared for the later electrochemical analysis. After every 24 h of electrolysis, the Mn^{2+} and Pb^{2+} concentrations of electrolyte samples were measured by inductively coupled plasma mass spectrometry (ICP-MS, AGILENT 7500), and the internal isotopic standards were 10 ng/mL In for Mn^{2+} and 10 ng/mL Bi for Pb^{2+} , respectively. And, the η_{MnO_2} values were

calculated by Faraday's law. The corresponding electrolyte samples were measured by Malvern laser particle size analyzer (MS 2000) to obtain the particle size distribution of suspended anode slime. Moreover, the anode slime detached from the substrate was collected from turbid electrolyte by a suction flask. And, the quality of detached anode slime was determined by heating at 120 °C to constant weight. The change of MnO_4^- ions was observed spectrophotometrically by pipetting out electrolytes at initial electrolysis time intervals and measuring the change in the absorbance at 525 nm. The above solution samples were determined three times to ensure the stability of the data. And, the error bars represented the standard deviation of three independent tests, which were listed in the figures.

Electrochemical measurements

The electrochemical experiments including cyclic voltammetry (CV) measurements and linear sweep voltammetry (LSV) tests were performed on a CHI608D electrochemistry workstation (Shanghai Chenhua, China) using a three-electrode system. For all the measurements, the anode samples with a geometric area of 1 cm² were used as the working electrodes after specific polarization time (24, 48, 72, and 240 h). Meanwhile, aluminum sheets with a geometric area of 1.5 cm² were used as the counterelectrodes, and the reference electrode was a saturated mercurous sulfate electrode (MSE). All the measurements were performed in a synthetic electrolyte of 45 g/L Zn^{2+} and 150 g/L H_2SO_4 at 35 ± 1 °C. The scanning range of CV was from -1.4 to 1.6 V at a constant scan rate of 1 mV/s, and the initial potential was -1.4 V. To improve the visual representation of CV curves in this paper, all images were cropped to a range from -1.4 to 1.4 V for direct comparison. For LSV, the potential was scanned from 1.0 to 1.5 V for anodic potentiodynamic polarization with a constant scan rate of 1 mV/s. Unless mentioned otherwise, all the potentials were recorded with respect to the MSE.

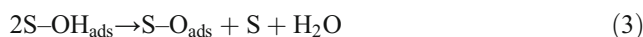
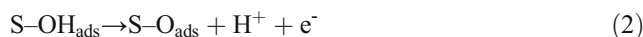
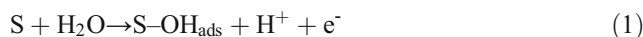
Deposit examination

After 240 h of electrolysis, deposits of anode surface were dried at room temperature and prepared for tests of morphology and phase composition. The morphology of the anode surface was examined by a scanning electron microscope (SEM, Qunata FEG 250) to obtain high-resolution images. X-ray diffraction (XRD, Rigaku Ultima IV) was used to analyze phase composition. The scanning rate during the XRD was kept at 10°/min within the scanning range of 20°–70° (2-theta).

Results and discussion

Analysis of kinetic parameters for OER

Steady polarization curves were performed in the absence and presence of Mn^{2+} to obtain kinetic parameters for OER. A widely approved mechanism for OER on active metal oxide electrodes could be proposed as the following reaction steps (Aromaa and Foese 2006).



Where, S and S-OH_{ads} represented the active site on the electrode surface and adsorption intermediate, respectively. Based on this mechanism, the rate determination step for a specific electrode was normally judged by the corresponding Tafel slope of OER. And for the lead-based electrode, the rate determination step could generally be determined by that when the Tafel slope b was ≥ 120 mV/dec, the formation and adsorption of S-OH_{ads} (step (1)) was rate determining; when b was ~ 40 mV/dec, the rate determination step was suggested to be steps (2) and (3); and when b was ~ 15 mV/dec, the generation of O_2 (step (4)) was rate determining.

In this research, the anodic kinetic parameters for lead-based anodes were determined from the anodic polarization curves (Fig. 1) using the Tafel formula (Xu et al. 2012).

$$\eta = a + b \log j \quad (5)$$

Where, η (under specific current densities $j = 0.045$ A/cm²) and j represented the overpotential and the corresponding

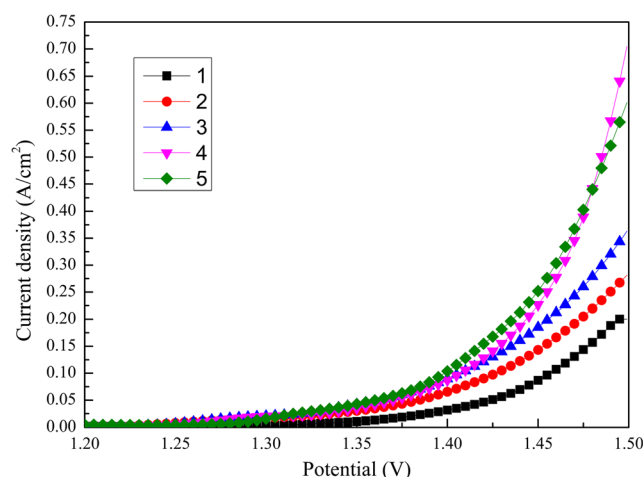


Fig. 1 Effect of Mn^{2+} on the anodic polarization on the fresh lead-based anodes with various concentrations: (1) blank, (2) 1 g/L, (3) 3 g/L, (4) 5 g/L, and (5) 10 g/L.

current density for OER, and b was the constant obtained by linear fitting of the relationship curve of η and $\log j$ in Origin 8.5.1 software. The exchange current density j_0 was calculated using the Tafel Eq. (5) when $\eta = 0$.

$$\log j_0 = -\frac{a}{b} \tag{6}$$

And, the transfer coefficient β was determined by Eq. (7) (Yang et al. 2013)

$$\beta = \frac{2.3RT}{b_a F} \tag{7}$$

Where, b_a was the corresponding Tafel slope at anodic polarization. And, R was the gas constant (8.314 J/(mol·K)), T was the thermodynamic temperature, and F was the faraday constant (96,500 C/mol). The values of b_a , η , β , and j_0 were given in Table 1. It was clear that the Tafel slopes markedly decreased from 135 to 117 mV/dec with the addition of Mn^{2+} . And, the noticeable increase of the exchange current densities (from 1.67 to 2.79×10^{-8} A/cm²) and transfer coefficients (from 0.444 to 0.513) was also found.

Generally, higher values of j_0 and β implied that the electrode was not easily polarizable, that electrode reversibility was improved, and that the electrode reaction easily occurred. Within the potential scan range (Fig. 1), the OER was the main reaction inevitably accompanied by the partial current for the Mn^{2+}/Pb^{2+} oxidation (remained very low about 1 mA/cm²) (Cachet et al. 1996). Therefore, this depolarizing effect indicated that the rate of OER was affected strongly by the existence of Mn^{2+} . Furthermore, this positive effect of Mn^{2+} on OER was ascribed to the formation of MnO_2 particle onto the anode surface, which was confirmed by its phase composition analysis (Fig. 6). However, this promotion effect approached saturation at a higher concentration of Mn^{2+} (up to 10 g/L), which suggested the limitation of active sites induced by the oxidation of Mn^{2+} on the anode surface. Throughout the experiments, the Tafel slopes all presented around 120 mV/dec, which indicated that the OER was controlled by step (1) according to the above proposed mechanism. This revealed the enhancement mechanism of the active site for OER, which played a key role in the electron transfer rate of step (1), since the promotion effect on OER is subject to the catalytic

properties and quantities of active sites. In this case, it could also explain the saturation observation obtained at high concentrations of Mn^{2+} due to the limited active sites induced by MnO_2 particles. Such saturation observation for OER indicated the optimization of Mn^{2+} concentrations as a feasible proposal in reducing energy consumption and avoiding consuming excessive amounts of manganese. Considering the competition mechanism among anodic reactions, this improvement for OER implied the potential in cutting down the generation of heavy metal anode slime.

This positive effect of Mn^{2+} on OER was proposed due to lack of further extension of the observation during a long period of zinc electrolysis (Zhang et al. 2009). In this work, a prolonged electrolysis (240 h) had been done on industrial lead-based anodes from zinc electrolyte as a function of Mn^{2+} concentration. The anodic kinetic parameters after the designed polarization time were listed in Table. 2, which were calculated from the polarization curves using the same method as described earlier. In particular, it presented two double-slope behaviors composed of distinct linear segments in the low-potential region (b_1) and high-potential region (b_2), which was regarded as the influence of partially evolved O_3 (Silva et al. 2003; Franco et al. 2006). Comparing the Tafel formula (5) with the Butler-Volmer formula in a high anodic polarization region ($\eta > 0.116$ V), the exchange current density j_0 was calculated in the low-potential region.

As shown in Table 2, the positive effect for OER among all the cases was further enhanced with a prolonged electrolysis, which was confirmed by the increase of j_0 values. In the electrolyte without Mn^{2+} , the values of j_0 increased from 1.67×10^{-8} to 1.30×10^{-5} A/cm² after 240 h of electrolysis. Although there was no apparent oxide layer formed on the anode surface (Fig. 2), this existential depolarization could be accounted for the catalytic effects of PbO_2 for OER (Zhang et al. 2017). And, what I found notable was the difference in promoting OER induced by the oxide layers formed in electrolytes of various Mn^{2+} concentrations. This positive effect was gradually strengthened in electrolytes of 1 (from 2.07×10^{-8} to 43.70×10^{-5} A/cm²) and 3 g/L Mn^{2+} (from 2.58×10^{-8} to 30.30×10^{-5} A/cm²). However, unstable fluctuations in j_0 were observed as the Mn^{2+} concentration increased to 10 g/L. The improvement of j_0 was reasonably ascribed to high effectiveness in improving the surface active

Table. 1 Effects of Mn^{2+} on initial kinetic parameters for anodic polarization on fresh lead-based anodes from the zinc electrolyte

Mn^{2+} (g/L)	Tafel slope, b_a (mV/dec)	Overpotential, η (mV)	Transfer coefficient, β	Anodic exchange current density, j_0 ($\times 10^{-8}$ A/cm ²)
0	135	868	0.444	1.67
1	129	817	0.465	2.07
3	124	774	0.484	2.58
5	118	734	0.509	2.71
10	117	726	0.513	2.79

Table 2 Effects of Mn^{2+} on kinetic parameters for anodic polarization on lead-based anodes after the designed electrolysis time points

Electrolysis time points, t (hours)	Mn^{2+} (g/L)	b_1	b_2	Anodic exchange current density, $j_0/(\times 10^{-5} \text{ A/cm}^2)$
24	0	0.2178	0.1453	2.98
	1	0.1069	0.3387	0.07
	3	0.1571	0.4500	2.21
	5	0.1432	0.4101	0.68
	10	0.1677	0.3898	2.89
72	0	0.2087	0.2665	3.97
	1	0.2346	0.3051	6.67
	3	0.1846	0.3672	2.98
	5	0.1605	0.3985	0.27
	10	0.1864	0.3867	0.61
240	0	0.1644	0.2756	1.30
	1	0.3332	0.4521	43.70
	3	0.3429	0.5310	30.30
	5	0.3040	0.4774	12.80
	10	0.2043	0.5045	3.20

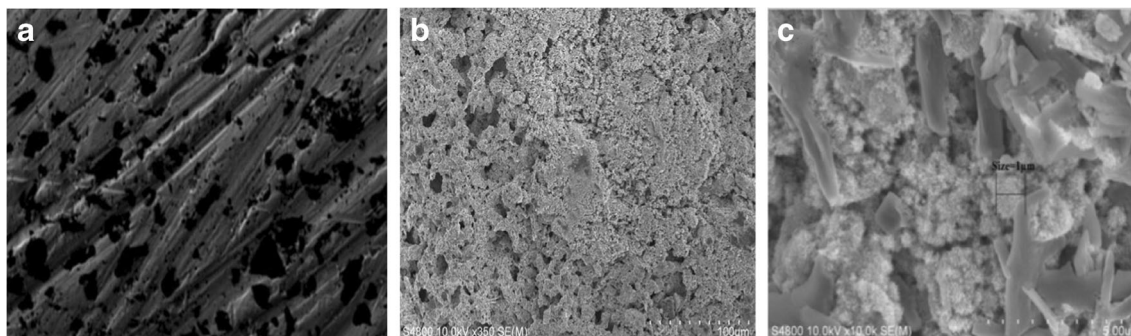
sites for OER induced by the gradual formation of oxide layers, and such differences in performance stability were speculated to be related to the microstructure of various oxide layers. Since previous investigations had revealed its significance in influencing the catalytic performance for OER (Mohammadi and Alfantazi 2015), such differences in the improvement for OER induced by the change of Mn^{2+} concentrations would be discussed in detail in the next section.

Microstructure and corrosion resistance of oxide layers

The SEM images of the fresh lead-based anodes and the same samples polarized for 240 h in the electrolyte without Mn^{2+} were shown in Fig. 2. For the fresh surface, whereas numerous cavities and deep holes were found, a relatively smooth and flat appearance was observed in Fig. 2a. After polarization for

240 h, although no apparent oxide layer with a certain thickness was formed on the anode surface (Fig. 2b), the surface defects were found to be partly repaired by the intricately woven vari-sized blocky oxide particles (Fig. 2c). This surface microstructure was loose and porous of which the packing particles were relatively small, even less than 1 μm . This implied that it could not provide sufficient corrosion resistance, which was quite consistent with the maximum dissolving of Pb shown in Fig. 5. The previous study had confirmed the enhanced effect of this surface microstructure on OER, which was mainly due to the electrocatalytic activity of $\beta\text{-PbO}_2$ (Silva et al. 2001; Zhong et al. 2014). Above all, no obvious anode slime was found in the electrolytic system, which revealed that the anode slime was mainly contributed by Mn^{2+} .

As Mn^{2+} ions were added into the electrolyte, obvious oxide layers were found to form on the anode surface in Fig. 3. And, the surfaces were also found to have suffered

**Fig. 2** Surface microstructure of lead-based anodes before (a) and after (b) and 240 h (c) electrolysis in the Mn^{2+} -free electrolyte

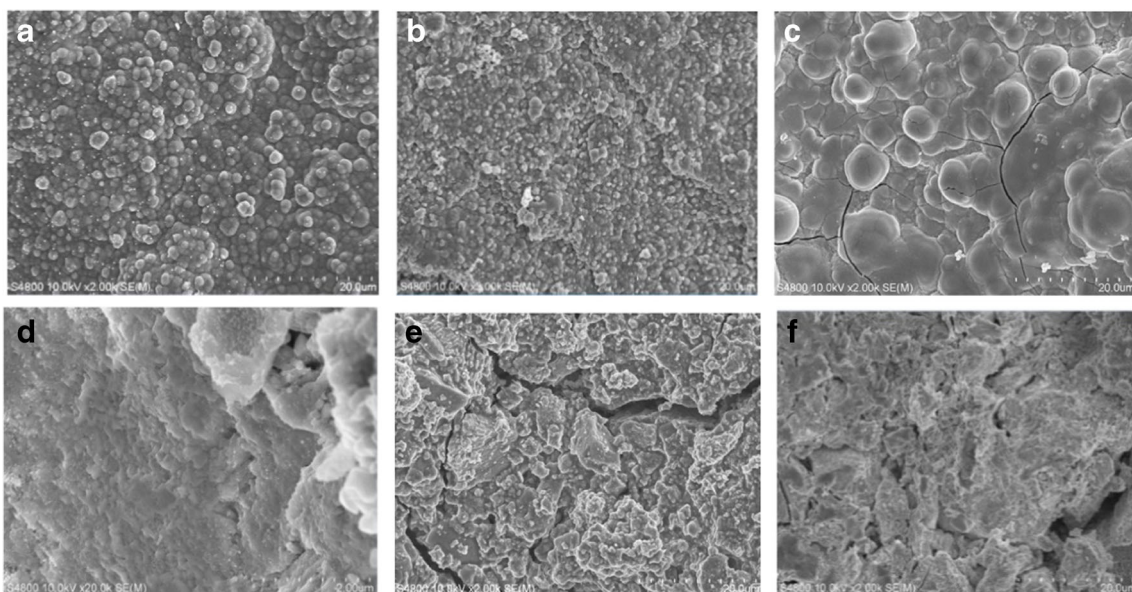


Fig. 3 Effect of Mn²⁺ on the surface morphology (×2000) of lead-based anodes after 240 h electrolysis: 1 g/L (a), 3 g/L (b), and 5 g/L (c): external layer 5 g/L (d): internal layer 10 g/L (e): external layer 10 g/L (f): internal layer

different levels of modification, implying these different efficiencies for promoting OER and corrosion resistance were introduced by various microstructures. While in the presence of either 1 or 3 g/L of Mn²⁺, the oxide layers represented were more compact, dense, and uniform (Fig. 3a and b). However, as the Mn²⁺ concentration increased to 5 and 10 g/L, oxide layers became thick, and even fell off in the local area of the anode surface. This caused the oxide layer to be divided into the external layer and the internal layer (Fig. 3c–e). The corresponding XRD analysis shown in Fig. 4 suggested that these oxide layers mainly consisted of α-MnO₂ and γ-MnO₂ accompanied by some few β-PbO₂, of which γ-MnO₂ was significantly represented because of its obvious characteristics of diffraction peaks at 2θ values of 22.2° and the sharper diffraction peak at 2θ values of 37.1°, 42.4°, and 56.1° nearby. And, γ-MnO₂ had been reported to possess better electrocatalytic and depolarization activity (Ye et al. 2015). Furthermore, the current peaks (b) of OER were larger on compact oxide layers formed in lower Mn²⁺ in Fig. 6, revealing its high potential in increasing activity sites and thereby enhancing the stimulated rate of OER. And, the enhanced change of oxide layers in adhesiveness was also partly supported by CV analysis (Fig. 6), showing the obvious intensity increase of peaks (d) assigned to the reduction of MnO₂ on the anode surface with the decrease of Mn²⁺. For this oxide layer, previous investigations had revealed its effectiveness in preventing the dissolution of lead-based anodes, which was mainly determined by its structure compactness and adhesiveness (Jaimes et al. 2015). In this work, the weakening tendency of peaks (a) assigned to the dissolution of Pb was also observed with the decrease of Mn²⁺, indicating the advantage of the oxide layer

obtained in low Mn²⁺ to promote corrosion resistance. This was further confirmed by the fact that Pb²⁺ concentrations in electrolytes decreased as the reduction of Mn²⁺ shown in Fig. 5. It represented that Pb²⁺ concentrations were controlled around 0.5 mg/L in the presence of either 1 or 3 g/L Mn²⁺. Whereas, the more fluctuant Pb (0.5–1.5 mg/L) was observed with Mn²⁺ concentrations ≥ 5 g/L. Such improvement of corrosion resistance induced by oxide layers formed in lower Mn²⁺ concentrations provided a feasible alternative in reducing and controlling lead contamination of zinc electrolysis industry from the source. And, it also implied the enormous potential in decreasing the consumption of manganese resources.

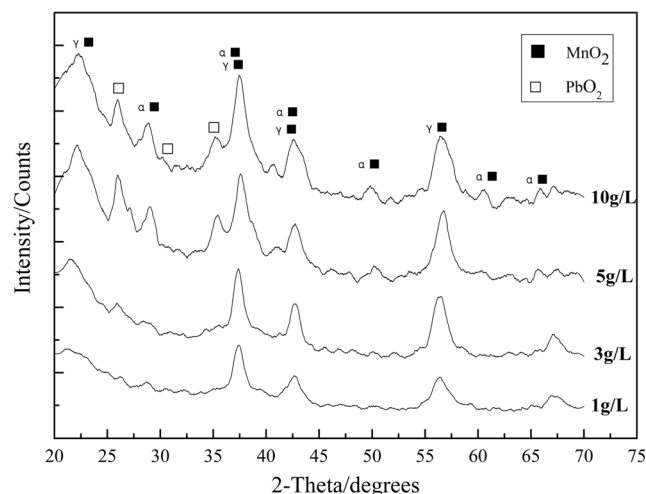


Fig. 4 XRD patterns of the oxide layers corresponding to Fig. 3

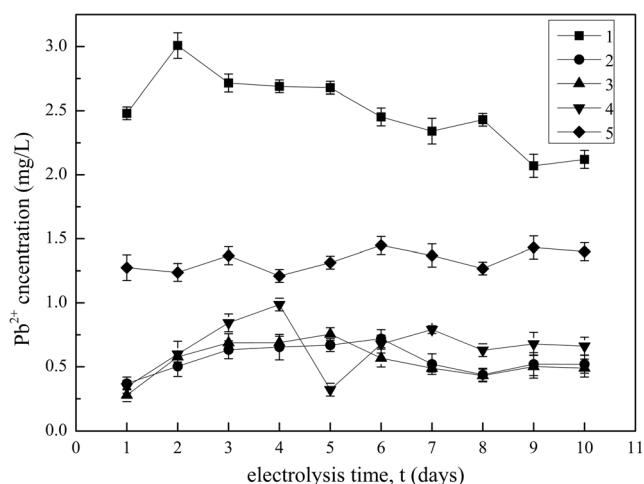


Fig. 5 The trend of lead content in electrolytes as a function of time in the presence of Mn^{2+} : (1) blank, (2) 1 g/L, (3) 3 g/L, (4) 5 g/L, and (5) 10 g/L. The error bars represented the standard deviation of three independent measurements for each sample

Altamari et al. had reported that the morphology of electro-deposits was mainly determined by the ratio between nucleation rate and growth rate of nucleated particles, which was significantly affected by the concentration of the precursor metal ion (Altamari and Pagnanelli 2016). Based on the nucleation thermodynamics of metals (Martin 2010), we could draw the following conclusions: (i) the fluctuation of the precursor metal ion concentration was one of the main driving forces of the nucleation process; (ii) compared with the growth of crystal nucleus, more energy was required in nuclei formation due to the increase of surface free enthalpy caused by the phase transition. In case of lower Mn^{2+} , the appropriate fluctuation of Mn^{2+} concentrations kept the new crystal nucleus continuously generating, matching well with the growth rate

of nucleated particles. The similar-sized particles formed in this case further agglomerated leading to the uniform and compact morphology of the oxide layer. Under high magnification in Fig. 3e and f, the crystalline particles became distinctly large and thick and arranged with disorganized overlaps. As a consequence, it led to the masking of active sites on the reaction interface weakening the positive effect of active particles on OER. Such adverse change of microstructure in the presence of higher Mn^{2+} concentration reflected the results of grain coarsening caused by the too large rate ratio (Fig. 6). It resulted in an increase in the cavities between particles, and thereby made the structure loose and unstable. Meanwhile, Pb was found to begin to largely enter into oxide layers by EDX analysis in Table 3. And, such oxide layers (especially the external layers) tended to fall off by the scour of the O_2 and electrolyte, increasing the risk to form anode slime containing abundant Pb.

Effect of Mn^{2+} on the generation of anode slime

In the past years, many literatures had focused on the key role of Mn^{2+} in influencing the OER and the microstructure of the oxide layers discussed above (Mohammadi and Alfantazi 2015; Jaimes et al. 2015). But, less attention was spent on its effect on the generation of anode slime. During the zinc electrolysis process, the overall anode oxidation reaction of Mn^{2+} had been previously reported to follow by Eq. (8) (Nijjer et al. 2000; Mahon and Alfantazi 2014).

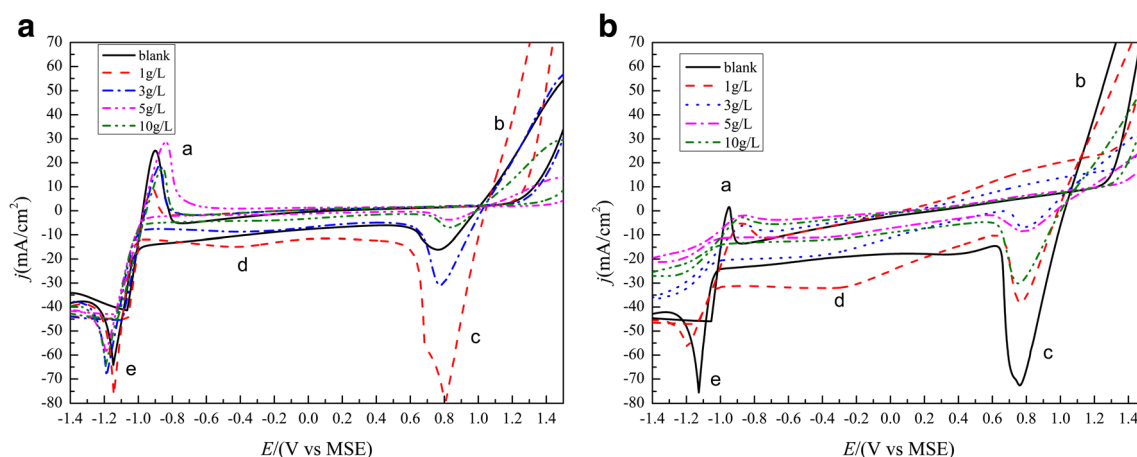
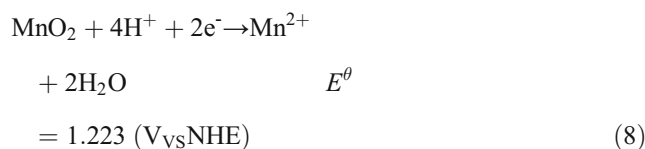


Fig. 6 The cyclic voltammetry (CV) curves of the lead-based anodes after 24 (a) and 240 h (b) polarization treatments from zinc electrolytes in the presence of Mn^{2+} : (1) 1 g/L, (2) 3 g/L, (3) 5 g/L, and (4) 10 g/L

Table. 3 EDX analysis corresponding to the oxide layers obtained from the SEM images in Figs. 3 and 4. All the analysis data correspond to an average of characteristic regions with areas of 100 μm² each on the sample surfaces

The electrolyte with various Mn ²⁺ concentrations	Molar composition (%)
Blank	O, 50.56; Pb, 48.97; Zn, 0.47
1 g/L	O, 71.33; Mn, 24.63; S, 1.68; Pb, 0.70; Zn, 1.66
3 g/L	O, 79.80; Mn, 16.90; S, 1.20; Pb, 1.50; Zn, 0.60
5 g/L: external layer	O, 65.60; Mn, 30.10; S, 1.90; Pb, 3.20; Zn, 0.20
5 g/L: internal layer	O, 73.10; Mn, 18.73; S, 2.45; Pb, 4.32; Zn, 0.40
10 g/L: external layer	O, 68.90; Mn, 25.10; S, 0.50; Pb, 4.90; Zn, 0.60
10 g/L: internal layer	O, 74.90; Mn, 15.10; S, 1.80; Pb, 7.90; Zn, 0.30

Clarke et al. (2006) had proposed that this anode oxidation process was mainly followed by the electrochemical-chemical-electrochemical mechanism in the acid sulfate solution, which was given by Eqs. (9)–(11).



As shown in Fig. 7, the minimum anode slime had been found in electrolyte of 10 g/L Mn²⁺. But, the most significant difference was that more than 90% of anode slime appeared in the electrolyte throughout the 240 h of electrolysis in electrolyte of 1 g/L Mn²⁺. Such results might seem counterintuitive. In “Microstructure and corrosion resistance of oxide layers,” it was stated that the loose and unstable oxide layers obtained in electrolyte of 10 g/L Mn²⁺ were more likely to fall off and resulted in excess anode slime. Therefore, such results were speculated to be correlated with the inherently different generation mechanism caused by the change of the Mn²⁺ concentration.

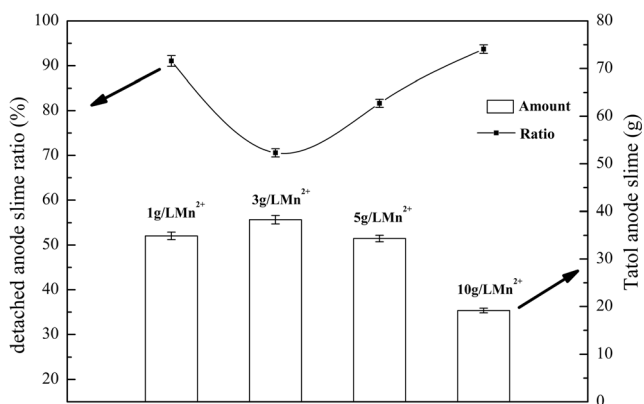
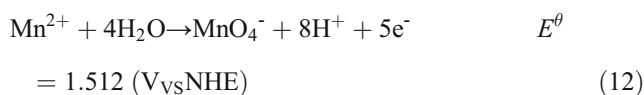


Fig. 7 Effect of Mn²⁺ on the quantity of anode slime (line) and the detached anode slime ratio (b) throughout the 240 h electrolysis experiments in the presence of Mn²⁺: (1) 1 g/L, (2) 3 g/L, (3) 5 g/L, and (4) 10 g/L. The error bars represented the standard deviation of three independent measurements for each sample

As also had been reported (Recéndiz et al. 2009), the generation of MnO₂ could be initiated by the formation of MnO₄⁻ at higher potentials (reaction (12)).



As shown in Fig. 8a, the MnO₄⁻ concentrations of the electrolytes obtained around reaction interface were found to notably increase along with the decrease of the Mn²⁺ concentration. In this case, it suggested that the reaction (12) took an increasingly dominant role in the initial electrochemical step of Mn²⁺ to MnO₂. This conclusion was further supported by the higher potentials caused by low concentrations of Mn²⁺ in Fig. 8b (Kelsall et al. 2000). Such results revealed that the generation mechanism of anode slime was fundamentally changed. In electrolytes of lower Mn²⁺ concentrations, the formation of Mn³⁺ intermediate (reaction (13)) was prone to occur in the bulk electrolyte because of the MnO₄⁻ ions diffusing away from the anode surface, and thereby to experience reactions (10) and (11) generates a large amount of suspended anode slime. Conversely, the reduction of anode slime at 10 g/L Mn²⁺ could be reasonably inferred to be due to the partial inhibition of excessive Mn²⁺ on the disproportionation of Mn³⁺ intermediate (reaction (10)), and the enhancement of OER induced by MnO₂ particles that adhered more rapidly to the anode surface.

As shown in Fig. 9, the η_{MnO₂} value was introduced to represent the generation amount of anode slime. The entire series of the η_{MnO₂} values were found to rapidly decrease with the extension of electrolysis, suggesting the positive role of oxide layers in cutting down anode slime. It was reasonably ascribed to the high effectiveness of MnO₂ particles in extending the surface active sites for OER. Thus, the accelerated formation and adsorption of intermediate MnO₂-OH_{ads} (step (1)) weakened the oxidation of Mn²⁺ competing with the OER. After being polarized for 240 h, the minimum η_{MnO₂} (approximately 1%) was obtained in the electrolyte of 3 g/L Mn²⁺, indicating the positive effect of compact and stable

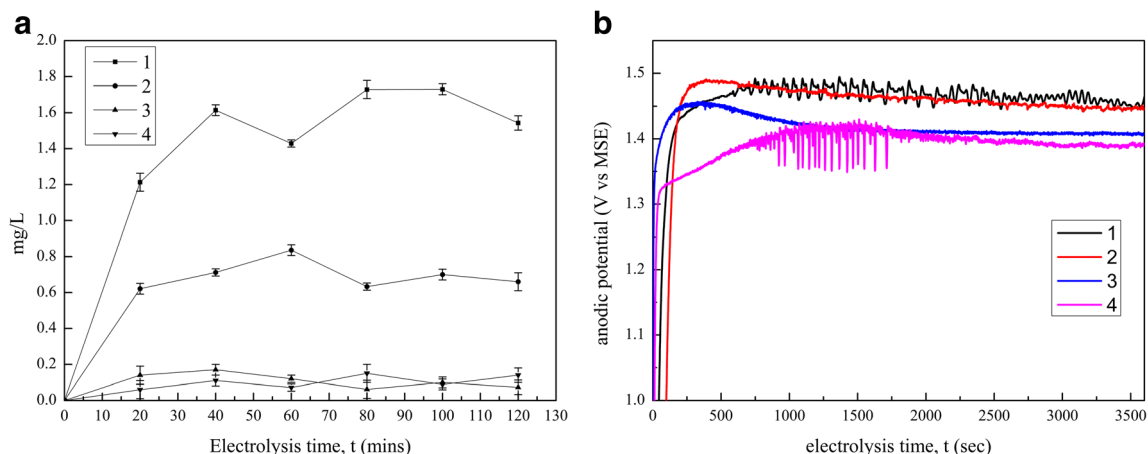


Fig. 8 The initial changes of MnO_4^- ions (a) and anodic potentials (b) obtained on the fresh lead-based anodes from zinc electrolytes in the presence of Mn^{2+} : (1) 1 g/L, (2) 3 g/L, (3) 5 g/L, and (4) 10 g/L. The

electrolyte samples were pumped from the electrolyte tightly around anode surfaces. The error bars represented the standard deviation of three independent measurements for each sample

oxide layers (Fig. 3b) on decreasing anode slime, and thereby implying the potential in optimizing Mn^{2+} concentration.

Actually, more urgent attention should be focused on the distribution characteristics of anode slime in zinc electrolysis industry because of its negative impact on the electrolytic environment, especially that the recycling of suspended anode slime in the zinc electrolysis system had always been a tough problem, leading to turbidity of the electrolyte and additional energy consumption (Moats 2008). As a favorable situation, anode slime was expected to settle rapidly to the bottom of cell and then be periodically removed. The Stoke law had revealed the essential effect of the particle size on its settling performance, which was consistent with the relationship between particle size and anode slime distribution in actual zinc electrolysis cell in Fig. 10. It indicated the advantages of larger particles in settlement, whereas smaller anode slime ($< 20 \mu\text{m}$)

was difficult to sink and mostly suspended in the upper electrolyte.

As shown in Fig. 9b, the red dotted line marked at the 100% of detached anode slime ratio represented the critical balance of the anode slime whether attached ($< 100\%$) or fell off ($> 100\%$) from the anode surface. The detached ratios always appeared around this critical ratio in electrolyte of 1 g/L Mn^{2+} , supporting the conclusion that most anode slime was generated and suspended among the electrolyte due to the change of initial electrochemical pathway (reaction (12)). And, this suspended anode slime which was sized mostly around $20 \mu\text{m}$ was found in Fig. 11, which indicated its poor settling performance. Thus, it revealed the potential risk that affected the quality of zinc products and increased the burden of electrolyte preparation (Ivanov and Stefanov 2002). For the particle size of electrodeposited MnO_2 , the previous literature

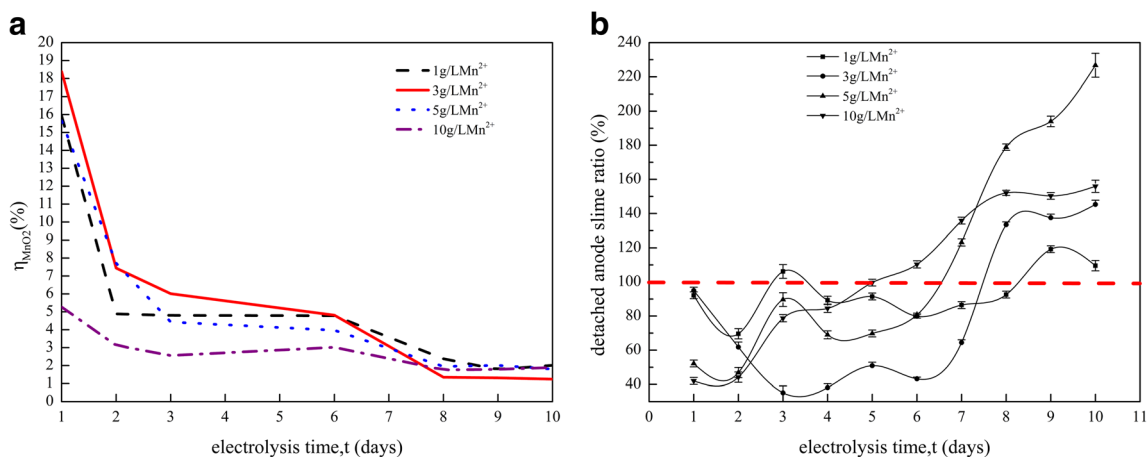
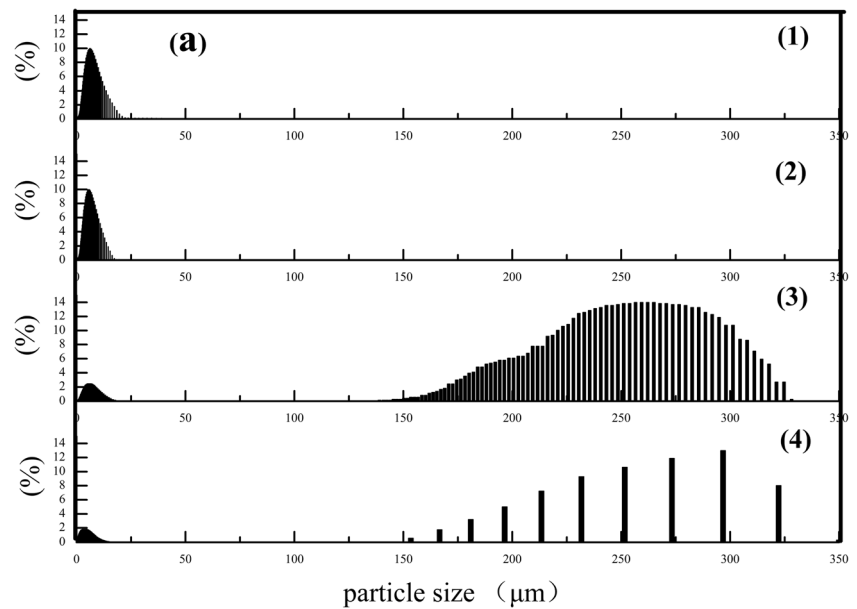


Fig. 9 Effect of Mn^{2+} on generation efficiency of anode slime (a) and the detached anode slime ratio (b) as a function of time in the presence of Mn^{2+} : (1) 1 g/L, (2) 3 g/L, (3) 5 g/L, and (4) 10 g/L. The error bars represented the standard deviation of three independent measurements for each sample

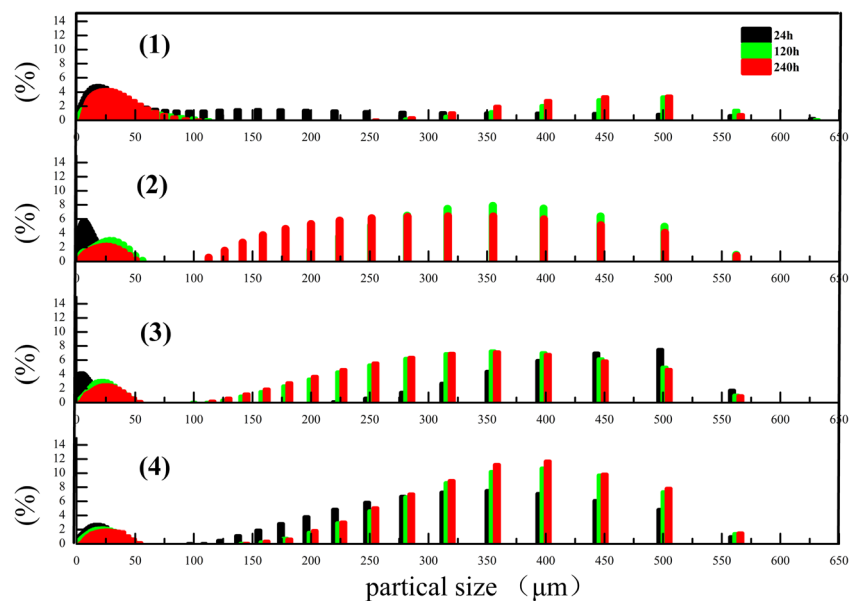
Fig. 10 The particle size distribution of suspended anode slime in various cell depths during actual zinc electrolysis production process: (1) 0–16 cm; (2) 16–32 cm; (3) 32–48 cm; (4) 48 cm, bottom of cell



had indicated that it was mainly affected by its nucleation and nucleus growth, which was dominated by the supersaturation of Mn^{4+} (Maphanga et al. 2009). Therefore, such results could be ascribed to the fact that (i) higher potentials (Fig. 8b) as driving force accelerated the formation rate of the small primary nucleus and (ii) the growth of nucleated particles occurred in liquid system (reactions (13) and (11)) was hindered by the disturbance of bubbles and fluid. After 240 h of electrolysis, the proportion of the larger suspended anode slime was found to markedly increase in the electrolyte of 3 g/L Mn^{2+} , which suggested the positive induction of compact

oxide layers in the initial change of Mn^{2+} oxidation pathway. This could be due to its significant improvement for anode potentials (Jaimes et al. 2015). But, this positive role had less influence in the case of electrolyte of 1 g/L Mn^{2+} that particles with a size of 50 μm still occupied a considerable proportion after 240 h of electrolysis. Moreover, for the electrolyte of 10 g/L Mn^{2+} , the larger proportion of detached ratio values in later electrolysis (Fig. 9b) indicated the propensity of early anode slime in generation site, which tended to adhere onto the anode surface relatively quickly. This attachment tendency of MnO_2 particles displayed high capacity in inhibiting further

Fig. 11 The particle size distribution of suspended anode slime in the zinc electrolyte as a function of time in the presence of Mn^{2+} : (1) 1 g/L, (2) 3 g/L, (3) 5 g/L, and (4) 10 g/L



generation of anode slime (Fig. 7). However, the corresponding oxide layers were prone to overthickness and unstable (Fig. 3c and e). And, its random detachment also caused the significant increase in particle size of anode slime in the electrolyte (from 200 to 550 μm). As such, it revealed high potential of a reasonable adjustment of Mn^{2+} concentration in improving the settling performance of the anode slime.

Conclusion

In order to reduce the heavy metal anode slime and thereby optimize its properties without introducing additional resources and energy consumption during zinc electrolysis industry, the role of Mn^{2+} ions on the generation of anode slime was investigated in detail. The Mn^{2+} was discovered to significantly promote OER, inhibit η_{MnO_2} , and weaken the dissolution of Pb, suggesting promising potential of the regulation of Mn^{2+} concentration on achieving the control of heavy metal anode slime more eco-friendly. Kinetic analysis indicated the controlled step for promoting OER which was the formation and adsorption of the intermediate $\text{MnO}_2\text{-OH}_{\text{ads}}$. The significant improvement was found in electrolytes of 1 and 3 g/L Mn^{2+} , but became unstable as the Mn^{2+} concentration increased to 10 g/L. This result was correlated with much different properties of oxide layers that its changes of microstructure are involved in, as it confirmed that the positive role of compact oxide layers in contributing to high corrosion resistance and activity for OER, but higher Mn^{2+} resulted in its micro-morphology of overthickness and instability. Such differences resulted from the effect of the Mn^{2+} concentration fluctuation on kinetic rates of the nucleation growth process. The generation mechanism of anode slime was found to be changed in essence due to varying Mn^{2+} concentrations, revealing that the root cause of excessive suspended anode slime was the change of the initial pathway of Mn^{2+} electro-oxidation. As such, the smaller particle (around 20 μm) of anode slime obtained in lower Mn^{2+} was mainly ascribed to nucleation sites transferred into the liquid system. Higher Mn^{2+} indicated great potential in improving the settling performance of anode slime, whereas the positive role of oxide layers was weakened by the adverse change of microstructure. This investigation should help improve the generation of anode slime in a much cleaner way for the zinc electrolysis industry.

Funding information This work was supported by the National Key R&D Program of China (2017YFC0210402), National Major Science and Technology Program for Water Pollution Control and Treatment (2017ZX07402004), Natural Science Foundation of China (51304178, 41673114), and the Central Level, Scientific Research Institutes for Basic R&D Special Fund Business (Chinese Research Academy of Environmental Sciences, 2016YSKY034, 2016YSKY-015), and by Funds of State Key Laboratory of Environmental Criteria and Risk Assessment (SKLECRA201754).

References

- Adcock PA (2017) Zinc electrowinning in the presence of iron (II). *J Entomol* 48(1):25–35
- Alamdari EK, Darvishi D, Khoshkhou MS, Javid FA, Marashi SPH (2012) On the way to develop co-containing lead anodes for zinc electrowinning. *Hydrometallurgy* s119–120(5):77–86. <https://doi.org/10.1016/j.hydromet.2012.01.009>
- Alkatsev VM, Alkatsev MI, Lin KVA, Darchiev IV (2014) Influence of impurities in electrolyte (tin, germanium, and antimony) on current efficiency within electrowinning of zinc. *Russ J Non-Ferrous Met* 55(4):327–330. <https://doi.org/10.3103/S1067821214040026>
- Alkatsev VM, Alkatsev MI, Darchiev IV, Linkov VA (2015) Certain peculiarities of the influence of antimony on electrolysis parameters of zinc. *Russian J Non-Ferrous Met* 56(6):611–614. <https://doi.org/10.3103/S1067821215060024>
- Altamari P, Pagnanelli F (2016) Electrochemical nucleation and three-dimensional growth of metal nanoparticles under mixed kinetic-diffusion control: model development and validation. *Electrochim Acta* 206:116–126. <https://doi.org/10.1016/j.electacta.2016.04.094>
- Aromaa J, Foesen O (2006) Evaluation of the electrochemical activity of a Ti-Ru O_2 -TiO₂ permanent anode. *Electrochim Acta* 51(27):6104–6110. <https://doi.org/10.1016/j.electacta.2005.12.053>
- Cachet C, Rerolle C, Wiart R (1996) Kinetics of Pb and Pb-Ag anodes for zinc electrowinning-II. Oxygen evolution at high polarization. *Electrochim Acta* 41(1):83–90. [https://doi.org/10.1016/0013-4686\(95\)00281-1](https://doi.org/10.1016/0013-4686(95)00281-1)
- Cachet C, Pape-Rérolle CL, Wiart R (1999) Influence of Co^{2+} and Mn^{2+} ions on the kinetics of lead anodes for zinc electrowinning. *J Appl Electrochem* 29(7):811–818. <https://doi.org/10.1023/A:1003513325689>
- Clarke CJ, Browning GJ, Donne SW (2006) An RDE and RRDE study into the electrodeposition of manganese dioxide. *Electrochim Acta* 51(26):5773–5784. <https://doi.org/10.1016/j.electacta.2006.03.013>
- Franco DV, Silva LM, Jardim WF (2006) Influence of the electrolyte composition on the kinetics of the oxygen evolution reaction and ozone production processes. *Braz Chem Soc* 17:746–757
- Houlachi G, Ghali E, Li X, Lafront A, Wei Z (2015) Influence of silver content on corrosion resistance of lead anodes during potential decay by electrochemical noise measurements. *Innov Corros Mater Sci* 5:43–52
- Ivanov I (2004) Increased current efficiency of zinc electrowinning in the presence of metal impurities by addition of organic inhibitors. *Hydrometallurgy* 72(1):73–78. [https://doi.org/10.1016/S0304-386X\(03\)00129-4](https://doi.org/10.1016/S0304-386X(03)00129-4)
- Ivanov I, Stefanov Y (2002) Electroextraction of zinc from sulphate electrolytes containing antimony ions and hydroxyethylated-butylene-2-diol-1, 4: part 3. The influence of manganese ions and a divided cell. *Hydrometallurgy* 64(3):181–186. [https://doi.org/10.1016/S0304-386X\(02\)00039-7](https://doi.org/10.1016/S0304-386X(02)00039-7)
- Jaimes R, Miranda-Hernández M, Lartundo-Rojas L, González I (2015) Characterization of anodic deposits formed on Pb-Ag electrodes during electrolysis in mimic zinc electrowinning solutions with different concentrations of Mn (II). *J Hydrometall* 156:53–62. <https://doi.org/10.1016/j.hydromet.2015.05.008>
- Kelsall G, Guerra E, Bestetti M (2000) Effects of manganese (II) and chloride ions in zinc electrowinning reactors. *Proc Electrochem Soc* 14:350–361
- Krause B, Sandenbergh RF (2015) Optimization of cobalt removal from an aqueous sulfate zinc leach solution for zinc electrowinning. *Hydrometallurgy* 155:132–140. <https://doi.org/10.1016/j.hydromet.2015.05.001>
- Lai YQ, Li Y, Lv XJ, Li J, Liu YX (2011) Electrochemical performance of a Pb/Pb-MnO₂ composite anode in sulfuric acid solution containing Mn^{2+} . *Hydrometallurgy* s115–116(4):64–70

- Lins VDFC, Abelha R, Castro MDMRD, Souza MMDD, Moraes LLD (2010) Effect of iron on energy consumption and current efficiency of zinc electrowinning from sulfate solution. *Tecnol Met Mater Mineração* 7(1–2):61–66. <https://doi.org/10.4322/tmm.00701011>
- Liu CX, Shen QF, Xiong M, Shan Y, He SF (2011) Inhibition behaviour of a mixed additive upon zinc electrowinning from sulphate solutions containing germanium. *Adv Mater Res* 291–294:1479–1483. <https://doi.org/10.4028/www.scientific.net/AMR.291-294.1479>
- Liu Z, Yu X, Xie G, Lu Y, Hou Y (2012) Influence of nickel on cathode process of zinc electrowinning. *Hydrometallurgy* 125–126(s125–126):29–33. <https://doi.org/10.1016/j.hydromet.2012.05.002>
- Liu JH, Chen BM, Guo ZC, Zhang YC, Xu RD (2013) Effect of the current density on oxygen overpotential and corrosion rate of the Al/Pb-Ag-Co anodes for zinc electrowinning. *Adv Mater Res* 634–638(1):1718–1723. <https://doi.org/10.4028/www.scientific.net/AMR.634-638.1718>
- Mahon M, Alfantazi A (2014) Manganese consumption during zinc electrowinning using a dynamic process simulation. *Hydrometallurgy* 150:184–191. <https://doi.org/10.1016/j.hydromet.2014.10.007>
- Maphanga RR, Parker SC, Ngoepe PE (2009) Atomistic simulation of the surface structure of electrolytic manganese dioxide. *Surf Sci* 603(21):3184–3190. <https://doi.org/10.1016/j.susc.2009.07.038>
- Martin G (2010) Reconciling the classical nucleation theory and atomic scale observations and modeling. *Adv Eng Mater* 8(12):1231–1236
- Moats MS (2008) Will lead-based anodes ever be replaced in aqueous electrowinning. *JOM* 60(10):46–49. <https://doi.org/10.1007/s11837-008-0135-7>
- Mohammadi M, Alfantazi A (2015) Evaluation of manganese dioxide deposition on lead-based electrowinning anodes. *Hydrometallurgy* 159:28–39
- Mohammadi M, Mohammadi F, Alfantazi A (2013a) Electrochemical reactions on metal-matrix composite anodes for metal electrowinning. *J Electrochem Soc* 160(4):35–43
- Mohammadi M, Mohammadi F, Houlachi G, Alfantazi A (2013b) The role of electrolyte hydrodynamic properties on the performance of lead-based anodes in electrometallurgical processes. *J Electrochem Soc* 160(3):27–33
- Moradkhani D, Rasouli M, Behnian D, Arjmandfar H, Ashtari P (2012) Selective zinc alkaline leaching optimization and cadmium sponge recovery by electrowinning from cold filter cake (CFC) residue. *Hydrometallurgy* 115–116(4):84–92. <https://doi.org/10.1016/j.hydromet.2011.12.021>
- Mureşan L, Maurin G, Oniciu L, Gaga D (1996) Influence of metallic impurities on zinc electrowinning from sulphate electrolyte. *Hydrometallurgy* 43(1–3):345–354. [https://doi.org/10.1016/0304-386X\(96\)00012-6](https://doi.org/10.1016/0304-386X(96)00012-6)
- Nijjer S, Thonstad J, Haarberg GM (2000) Oxidation of manganese and reduction of manganese dioxide in sulphuric acid. *Electrochim Acta* 46(2–3):395–399. [https://doi.org/10.1016/S0013-4686\(00\)00597-1](https://doi.org/10.1016/S0013-4686(00)00597-1)
- Recéndiz A, Nava JL, Lartundo-Rojas L, Almaguer I, González I (2009) Characterization of the corrosion layers electrochemically formed on the lead-silver/ H₂SO₄+Mn (II) interface. *J Electrochem Soc* 156(8):231–239
- Rerolle C, Wiart R (1995) Kinetics of Pb and Pb-Ag anodes for zinc electrowinning—I. Formation of PbSO₄ layers at low polarization. *Electrochim Acta* 40(8):939–948. [https://doi.org/10.1016/0013-4686\(95\)00026-B](https://doi.org/10.1016/0013-4686(95)00026-B)
- Shrivastava P, Moats MS (2009) Wet film application techniques and their effects on the stability of RuO₂-TiO₂ coated titanium anodes. *Appl Electrochem* 39(1):107–116. <https://doi.org/10.1007/s10800-008-9643-y>
- Silva LMD, Faria LA, Boodts JFC (2001) Green processes for environmental application. Electrochemical ozone production. *Pure Appl Chem* 73(12):1871–1884
- Silva LMD, Faria LA, Boodts JFC (2003) Electrochemical ozone production: influence of the supporting electrolyte on kinetics and current efficiency. *Electrochim Acta* 48(6):699–709. [https://doi.org/10.1016/S0013-4686\(02\)00739-9](https://doi.org/10.1016/S0013-4686(02)00739-9)
- Stefanov Y, Dobrev T (2013) Developing and studying the properties of Pb and TiO₂ alloy coated lead composite anodes for zinc electrowinning. *Trans IMF* 83(6):291–295
- Su C, Zhang W, Ghali E, Houlachi G (2017) Electrochemical investigation of electrolyte composition and electrolysis parameters during zinc electrowinning. *J Appl Electrochem* 47(8):941–958. <https://doi.org/10.1007/s10800-017-1091-0>
- Xu RD, Huang LP, Zhou JF, Zhan P, Guan YY, Kong Y (2012) Effects of tungsten carbide on electrochemical properties and microstructural features of Al/Pb-PANI-WC composite inert anodes used in zinc electrowinning. *Hydrometallurgy* s125–126(7):8–15. <https://doi.org/10.1016/j.hydromet.2012.04.012>
- Xu FY, Jiang LH, Li JH, Zou C, Wen XC, Zhang G, Li ZQ, Duan N (2016) Mass balance and quantitative analysis of cleaner production potential in a zinc electrolysis cellhouse. *J Clean Prod* 135:712–720. <https://doi.org/10.1016/j.jclepro.2016.06.147>
- Yang HT, Liu HR, Guo ZC, Chen BM, Zhang YC, Huang H, Li XL, Fu RC, Xu RD (2013) Electrochemical behavior of rolled Pb-0.8% Ag anodes. *Hydrometallurgy* 140:144–150
- Ye D, Wu T, Cao H, Wang Y, Liu B (2015) Electrocatalysis of both oxygen reduction and water oxidation using a cost-effective three dimensional MnO₂: graphene:carbon nanotube. *RSC Adv* 5(34):26710–26715. <https://doi.org/10.1039/C4RA14452J>
- Zhang QB, Hua Y (2009) Effect of Mn²⁺ ions on the electrodeposition of zinc from acidic sulphate solutions. *Hydrometallurgy* 99(3–4):249–254. <https://doi.org/10.1016/j.hydromet.2009.09.002>
- Zhang H, Li Y, Wang J, Hong X (2009) The influence of nickel ions on the long period electrowinning of zinc from sulfate electrolytes. *Hydrometallurgy* 99(1):127–130. <https://doi.org/10.1016/j.hydromet.2009.07.009>
- Zhang C, Xu Y, Lu P, Zhang X, Xu F (2017) Capillary effect-enabled water electrolysis for enhanced electrochemical ozone production by using bulk porous electrode. *J Am Chem Soc* 139(46):16620–16629. <https://doi.org/10.1021/jacs.7b07705>
- Zhong XC, Gui JF, Yu XY, Liu FY, Jiang LX (2014) Influence of alloying element Nd on the electrochemical behavior of Pb-Ag anode in H₂SO₄ solution. *Acta Phys -Chim Sin* 30(3):492–499
- Zhu J, Wu Y, Zuo J, Khan DF, Jiang C (2017) Effect of iridium(IV) ions on the electrowinning of zinc from acidic electrolytes. *Hydrometallurgy* 174:248–252. <https://doi.org/10.1016/j.hydromet.2017.04.010>